Supporting Information

In Situ Growth of Lead-Free Halide Perovskites into SiO_2 Sub-Microcapsules toward Water-Stable Photocatalytic CO_2 Reduction

Jie Liu[†a], *Ziho Wu*[†b], *Feng Zhang*[*a], *Mengzhen Zhao*[a], *Chao Li*[a], *Jie Li*[*b], *Bo Wen*[b], and *Feijiu Wang*[*a, c]

[a] Henan Key Laboratory of Photovoltaic Materials, Henan University, 1 Jinming Road, 475004 Kaifeng (China)

[b] School of Physics and Electronics, Henan University, 1 Jinming Road, 475004 Kaifeng (China)

[c] Center for Topological Functional Materials, Henan University, 1 Jinming Road, 475004 Kaifeng (China)

1. Experimental Section

1.1 Materials and Reagents

Cs(OAc) (99.9%), Ag(OAc) (99%), $Bi(OAc)_3$ (99.99%), 2,2'-bipyridine (bpy), $CoCl_2$, triethanolamine (TEOA), and acetonitrile were obtained from Sigma-Aldrich. Benzoyl bromide (>98%), cetyltrimethylammonium bromide (CTAB, 99%), tetraethylorthosilicate (TEOS, 99.9%), concentrated ammonia aqueous solution (25 wt%), lead(II) acetate trihydrate ($C_4H_6O_4Pb{\cdot}3H_2O$, 99.99%), and 1-octadecene (ODE, tech. 90%) were purchased from Aladdin Reagent Co. Ltd. Oleic acid (OA, tech. 90%), oleylamine (OAm, 90%) and cesium carbonate (Cs_2CO_3, 99.9%) were obtained from Adamas. Toluene (≥99.5%) was purchased from Luoyang Haohua Chemical Reagent Co. Ltd. Didecylamine (>97%) was purchased from Tokyo Chemical Industry (TCI). Anhydrous ethanol (98%), ethyl acetate, and methyl acetate (≥98%) were from Macklin.

1.2 Synthesis of $Cs_2AgBiBr_6$ Nanocrystals

The synthesis of $Cs_2AgBiBr_6$ nanocrystals was using a hot-injection method. Firstly, a mixture of Cs(OAc) (1 mmol), Ag(OAc) (0.5 mmol), and $Bi(OAc)_3$ (0.5 mmol), and 10 mL ODE together with 2.5 mL OA and 0.584 mL OAm was loaded in a 25 mL three neck round bottom flask equipped with a reflux condenser for 60 min at 100 °C under vigorous stirring. Then, benzoyl bromide precursor (390 μL) diluted in ODE was injected into the mixture under N_2. After 30 s, the reaction mixture was cooled by immersion in an ice-water bath. After cooling down, the resulting mixture was mixed with methyl acetate (anti-solvent), and centrifuged at 12000 rpm for 30 min, the supernatant was discarded and the precipitation was collected. The precipitated nanocrystals were re-dispersed in a mixed solution of toluene and methyl acetate and centrifuged at 12000 rpm for 20 min, and washed three times in this way. The final precipitation was collected and stored for characterization.

1.3 Preparation of Core-shell Mesoporous Sub-microspheres

1.3.1 Synthesis of Mesoporous Silica Hollow Sphere

Mesoporous silica hollow spheres were synthesized by following a previous work using a spontaneous self-transformation approach. [1] Typically, CTAB was dissolved in ethanol aqueous solution (50 mL water and 30 mL ethanol) containing concentrated ammonia aqueous solution (1 mL, 25 wt%). Then, the mixture was heated to 35 °C, and TEOS (1 mL) was rapidly added under vigorous stirring. After stirring at 35 °C for 24 h, the white product was collected by centrifugation at 4000 rpm for 10 min and washed three times with ethanol. The obtained white product was dispersed in water (300 mL) at 70 °C and stirred for 12 h to form mesoporous silica hollow spheres. The as-synthesized materials were transferred to an ethanol solution (120 mL) containing concentrated HCl (240 μL, 37%) and stirred at 60 °C for 3 h to remove the template CTAB. This process was repeated three times. At last, the precipitation was washed with anhydrous ethanol for three times again, and the final precipitation was dried to obtain mesoporous silica hollow spheres. The morphology and size of the product were characterized by scanning electron microscope (SEM) (Figure S1a,b). The size distribution (Figure S1c) shows a mean particle size of 460 nm. Furthermore, the Brunauer-Emmett-Teller (BET) analysis was performed to determine the specific surface area from the N_2 adsorption-desorption isotherms (Figure S1d). The pore size distribution was calculated to be ~ 2.9 ± 0.2 nm by the method based on nonlocal density functional theory (NLDFT). The synthesis of the mesoporous spheres with a mean particle size of 260 nm was using the same method except the amount of deionized water (~ 15 mL).

1.3.2 Preparation of $Cs_2AgBiBr_6$@SiO_2 Core-shell Mesoporous Microspheres

In a typical experiment, Cs(OAc) (96 mg, 0.5 mmol), $Bi(OAc)_3$ (97 mg, 0.25 mmol), Ag(OAc) (418 mg, 0.25 mmol), OAm (295 μL), ODE (5 mL) and OA (1.25 mL) were mixed in a 25 mL three-neck round-bottom flask. The mixture was heated to 100 °C under vacuum and stirred for 30 minutes. Mesoporous silica hollow spheres (15 mg) were dispersed into ODE, and then injected into the flask under N_2 atmosphere. The mixture was degassed and

dried by stirring for 1 h, then benzoyl bromides (195 μL) was quickly injected in N_2 atmosphere. After 15 s, the flask was immersed in an ice-water bath and cooled to room temperature. The crude reaction mixture was mixed with methyl acetate (anti-solvent), and centrifuged at 6000 rpm for 20 min. Then, the precipitation was collected and dispersed in a mixed solution of toluene and methyl acetate. After centrifuging at 2000 rpm for 10 min, the precipitation was remained after the process repeated twice. Finally, the precipitation was re-dispersed in toluene, centrifuged at 2000 rpm for 10 min, and washed repeatedly for 2 ~ 3 times to obtain the final product.

1.3.3 Preparation of $CsPbBr_3$@SiO_2 Core-shell Mesoporous Microspheres

In a 25 mL three-necked flask, lead(II) acetate trihydrate (60.8 mg) and cesium carbonate (16 mg) were suspended in 10 mL ODE. The reaction mixture was degassed at room temperature for 5 min and then heated to 115 °C for 60 min. Afterwards, a pre-dried OA (1.5 mL) and a didecylamine (1.25 mmol) were dissolved in 1 mL of toluene and then added under nitrogen atmosphere. After the complete dissolution of the metal precursors, the temperature of the reaction mixture decreased to 90 °C. Mesoporous microspheres (15 mg) were dispersed in dried ODE and put in the three-necked flask for 10 min. Then, 100 μL of a benzoyl bromide precursor diluted in dried ODE was injected into the mixture. The mixture was cooled down to room temperature after 15 s by using a water bath. Subsequently, a mixture of ethyl acetate and toluene (with a ratio of 6:1) was added into the crude solution to destabilize the colloids, and the product was collected by centrifugation at 4000 rpm for 10 min for 2 ~ 3 times. Then, the precipitation was dispersed in toluene, centrifuged at 2000 rpm for 10 min, and washed repeatedly for 2 times. Finally, the precipitation was collected and stored for characterization.

1.4 Characterization and Measurements

The optical absorption spectra were obtained using a UV/Vis/NIR spectrophotometer (Cary 5000). The photoluminescence (PL) and time-resolved PL (TRPL) spectra were recorded by a fluorescence spectrometer equipped with a Xenon lamp (FLS1000, Edinburgh Instruments Ltd., Edinburgh, UK). The variable temperatures were realized by a temperature controller. The PL lifetime measurements were recorded on the same spectrometer using a 375 nm picosecond pulsed diode laser as excitation light source. The phase purity of the final products was characterized by X-ray diffractometer (XRD) (Bruker D8 Advance, Bruker AXS Inc., Madison, USA) with Cu Kα radiation (λ = 1.54056 Å). Bright-field transmission electron microscopy (BF-TEM), high-resolution TEM (HR-TEM), high-angle annular dark-field-scanning TEM (HAADF-STEM) images, and energy-dispersive X-ray spectroscopy (EDS) analyses were collected by a JEM-F200 (JEOL, Japan) electron microscope with an accelerating voltage 200 kV. Scanning electron microscope (SEM) images were acquired on a JSM-7610F instrument (JEOL, Japan). X-ray photoelectron spectroscopy (XPS) measurements were performed in an analysis chamber (UHV−210−10 Torr during analysis) using a Versaprobe III-PHI Instrument (PHI, USA), and the core level binding energies of the different peaks were calibrated by setting the binding energy for C 1s at 284.6 eV. The N_2 adsorption-desorption isotherms were performed by a Micromeritics ASAP 2020M+C. Raman spectra were recorded by HORIBA LabRAM Odyssey microscopic Raman system using 785 nm excitation laser, with a grating of 1800 gr/mm.

1.5 Photocatalytic performance tests

To evaluate the photocatalytic activity for CO_2 reduction, 10 mg of catalysts was added into a gas-closed glass reactor (80 mL in capacity) containing 15 mg of 2,2'-bipyridine (bpy), 2 μmol of $CoCl_2$, 1.2 mL TEOA, 1.8 mL H_2O and 3.2 mL acetonitrile. High purity CO_2 was bubbled into the glass reactor with a flow rate of 40 sccm for 30 min to saturate the solution. After that, a 300 W Xe lamp with a 420 nm cut-off filter was used as the light source for the photocatalytic reactions. During the process, the reaction solution was stirred by a magnetic stirrer and maintains a constant reaction temperature of 25 °C by circulating cooling water. After each reaction, the gas product generated in the reactor was collected through a syringe and analyzed via gas chromatography (GC9790Ⅱ, Fuli, China)), equipped with a thermal conductivity detector and a flame ionization detector.

2. Computational Methods

We have used the CP2K [2] software package to perform all the density functional theory (DFT) calculations. The generalized gradient approximation (GGA), Perdew-Burke-Ernzerhof (PBE) [3] function, was adopted to describe the exchange and correlation interaction. The interaction between core and valence electrons was treated by norm-conserved Goedecker-Teter-Hutter (GTH) pseudopotentials [4] and the valence electron configurations of Cs ($5s^2 5p^6 6s^1$), Bi ($6s^2 6p^3$), Ag ($4d^{10} 5s^1$), Br ($4s^2 4p^5$), O($2s^2 2p^4$) and Si($3s^2 3p^2$) were considered. A 950 Ry cutoff energy was set for the plane wave part and a double-zeta Gaussian function with polarization (DZVP-MOLOPT) [5] was used to construct the Gaussian plane-wave mixed basis set. To include the long range dispersion interactions, we also added the Grimme DFT-D3 empirical correction [6]. The structures and atomic positions were fully relaxed until the change of forces on each atom was less than 0.05 eV/Å. Because of the large model size, we only considered the Γ point in reciprocal space sampling. To alleviate the mirror effect of its adjacent periodic structure, a 15 Å vacuum region was added above the heterojunction ($Cs_2AgBiBr_6$-SiO_2).

The double perovskite $Cs_2AgBiBr_6$ belongs to Fmm space group with face-centered cubic structure. Our calculated lattice constants is a = b = c = 11.23 Å, which agrees well with the reported 11.48 Å [7]. It has two possible surface structures with different surface-exposed atoms, namely surface termination of Bi, Ag, and surface termination of Cs. As reported [8], the latter has a lower surface energy comparing to the former one. Therefore, the termination of Cs was chosen as the exposed surface in our model. The most stable phase of SiO_2 is α-quartz and the calculated lattice constants is a = b = 4.89 Å, c = 5.41 Å, which is also in accordance with the reported [9] values (a = 5.05 Å, c = 5.54 Å). To model the $Cs_2AgBiBr_6$-SiO_2 heterostructure, we used two periodically layered (001) surface of $Cs_2AgBiBr_6$ and three periodically layered (0001) surface of α-quartz which exposed the terminated-O surface.

The adsorption energy (E_a) was calculated by:

$$E_a = E_{nH_2O-A} - E_A - nE_{H_2O}$$

Where n is the number of absorbed H_2O molecules and E_{nH_2O-A} is the optimized total energy of n H_2O on substrate. E_A is the total energy of optimized substrate ($Cs_2AgBiBr_6$ or $Cs_2AgBiBr_6$-SiO_2).

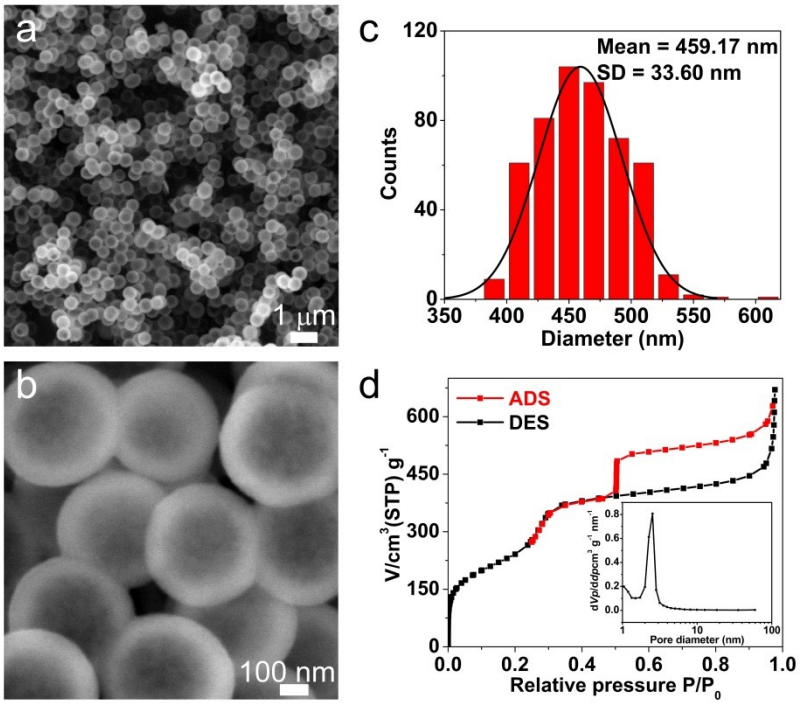

Figure S1. (a) and (b) exhibit the SEM images of mesoporous SiO_2 hollow spheres, (c) the size distribution, and (d) N_2 adsorption-desorption isotherm of SiO_2 and the insert gives the pore size distribution curve.

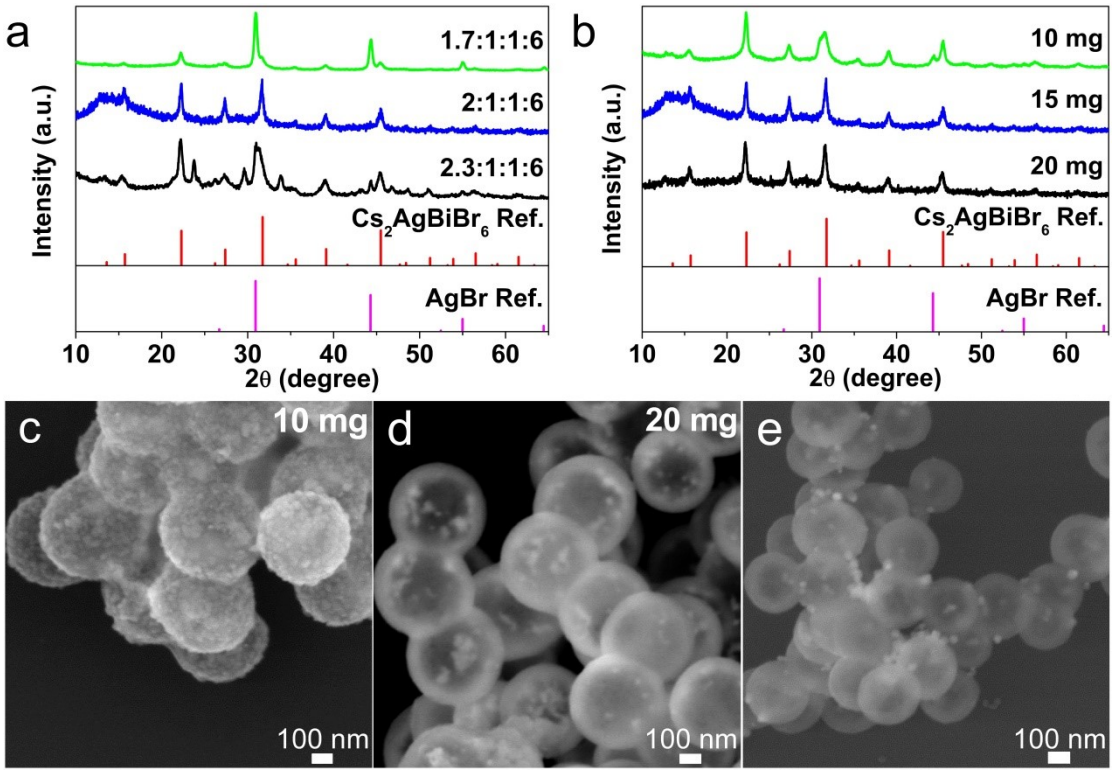

Figure S2. (a) The XRD patterns of $Cs_2AgBiBr_6@SiO_2$ (15 mg SiO_2 hollow spheres) by varying the ratio of Cs^+/Ag^+, (b) XRD patterns of the composites by adding the different amounts of SiO_2, (c)-(d) respectively present SEM images of the composites with different SiO_2 additives (10 mg and 20 mg), and (e) SEM image of $Cs_2AgBiBr_6@SiO_2$ by adding the undiluted benzoyl bromide.

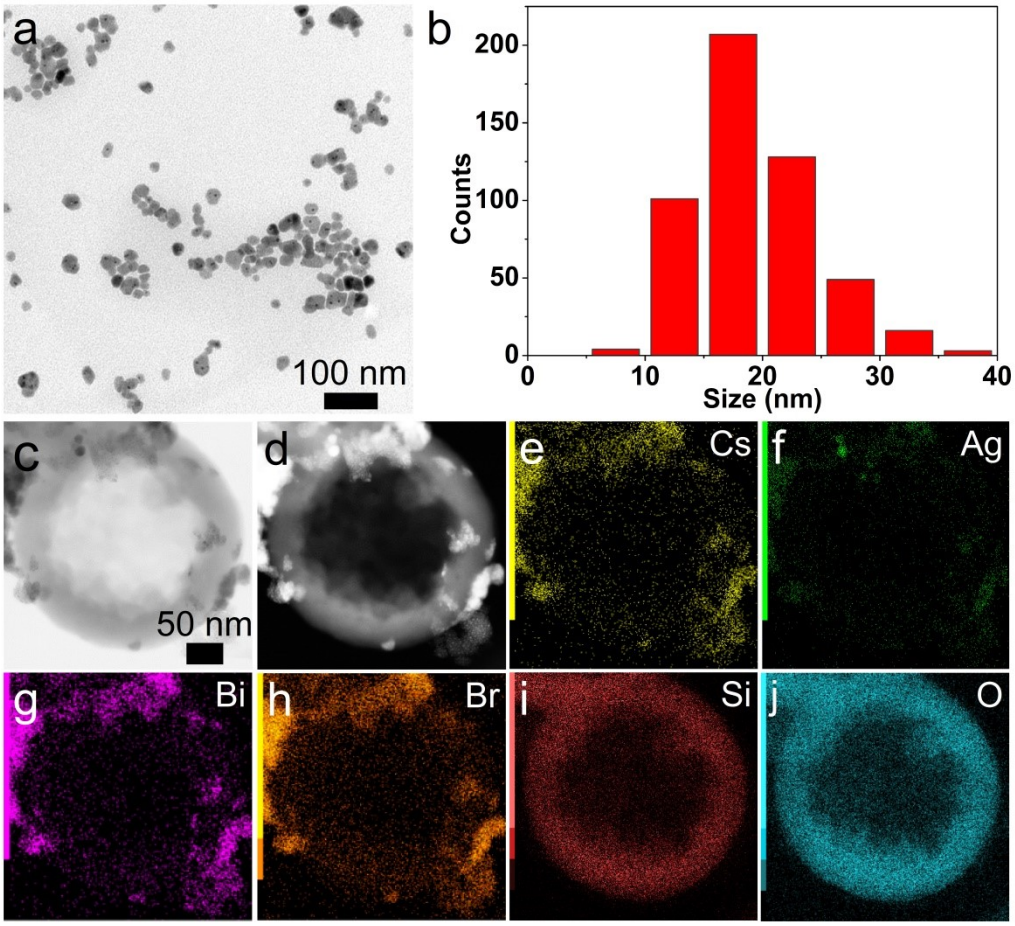

Figure S3. (a) BF-TEM image of $Cs_2AgBiBr_6$ nanocrystals in the supernatant, (b) the corresponding histogram of the size distributions, (c) BF-TEM image, (d) HAADF-STEM image, and the elemental mapping images of (e) Cs, (f) Ag, (g) Bi, (h) Br, (i) Si, and (j) O.

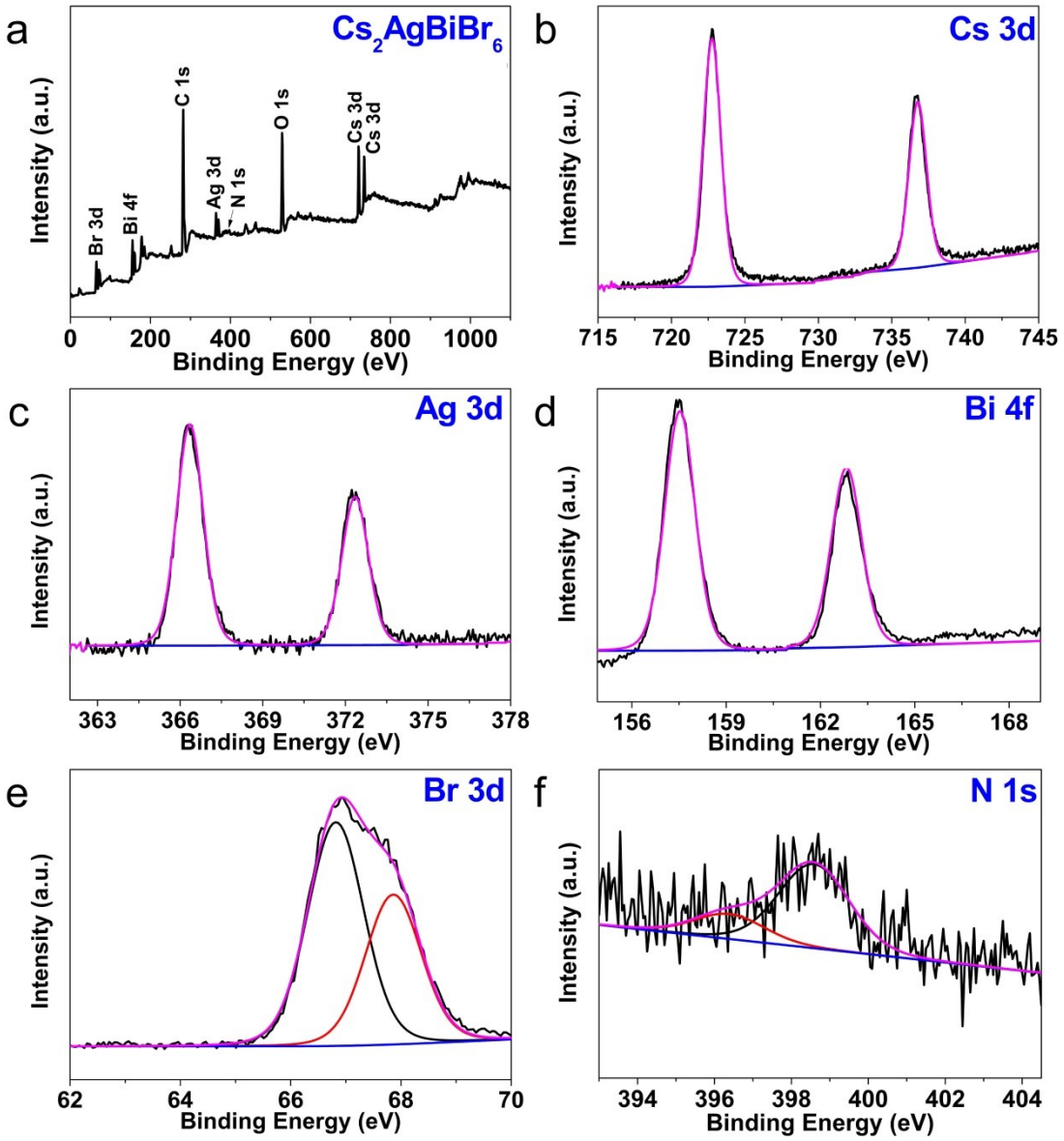

Figure S4. (a) The survey XPS spectra. The high-resolution XPS spectra of (b) Cs 3d, (c) Ag 3d, (d) Bi 4f, (e) Br 3d, and (f) N 1s regions of $Cs_2AgBiBr_6$ nanocrystals.

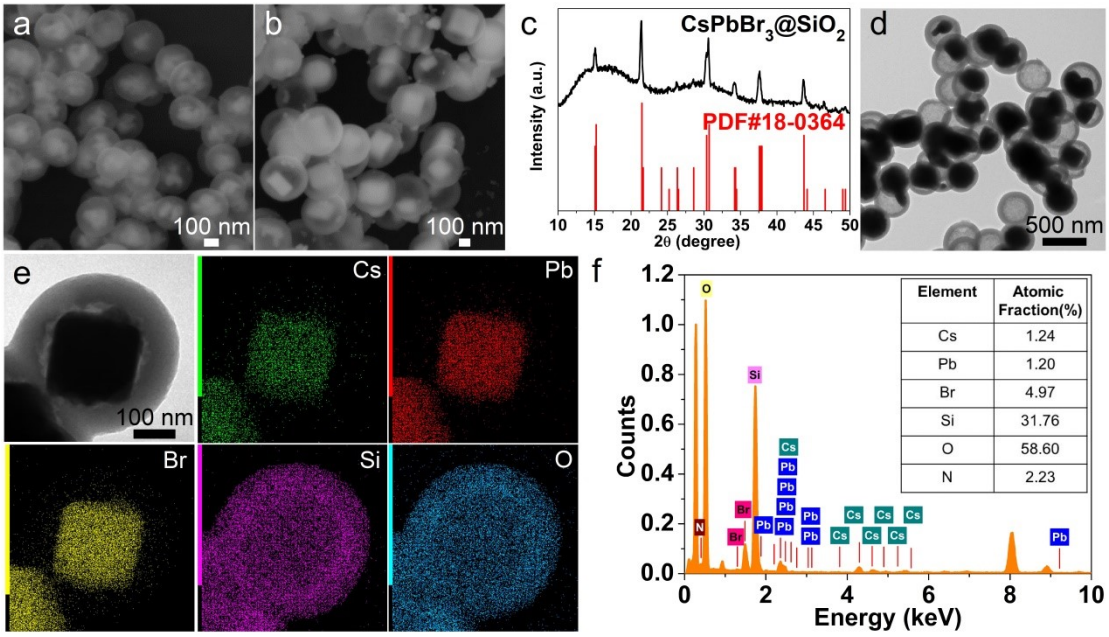

Figure S5. (a) SEM image of $Cs_2AgBiBr_6@SiO_2$ using SiO_2 hollow spheres with the diameter of 260 nm. (b) SEM image of $CsPbBr_3@SiO_2$. (c) XRD pattern of $CsPbBr_3@SiO_2$. (d) BF-TEM images of $CsPbBr_3@SiO_2$. (e) Elemental mapping images of Cs, Pb and Br elements dispersed in SiO_2, where the scale bar is 100 nm. (f) The corresponding EDS scanning results.

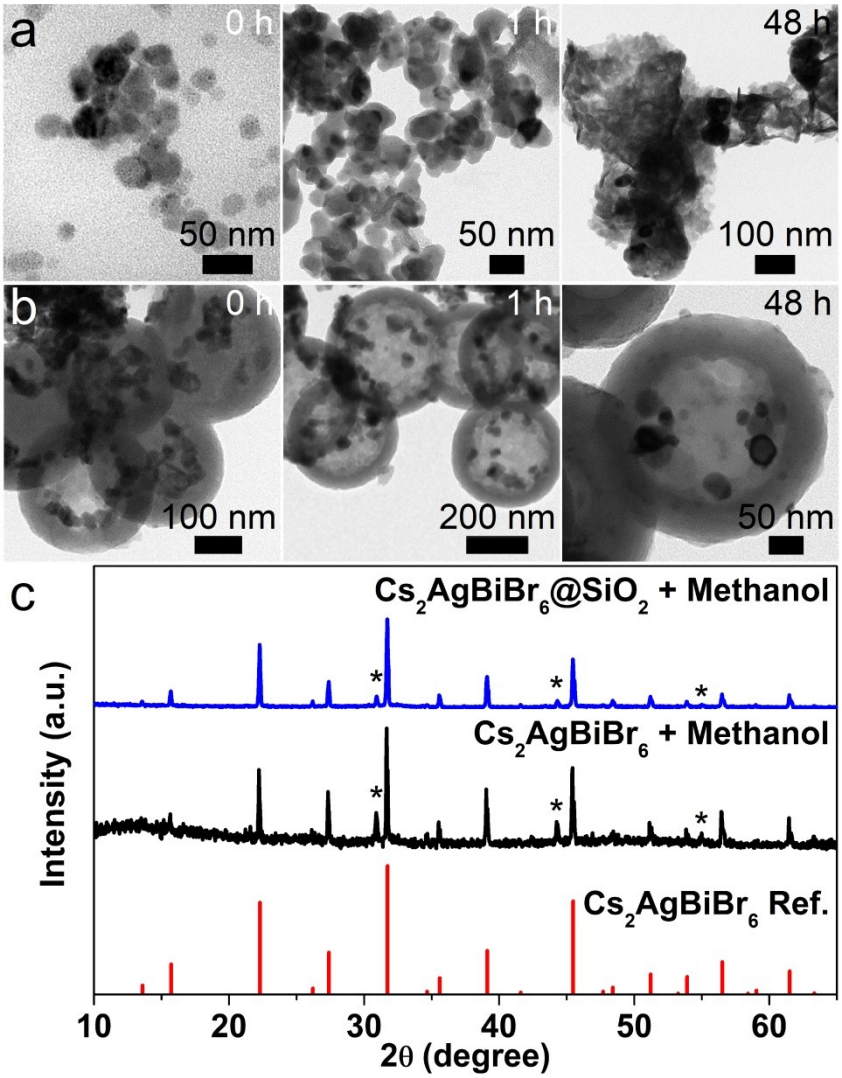

Figure S6. (a) BF-TEM images of $Cs_2AgBiBr_6$ nanocrystals with different storage time (0, 1, and 48 h) in methanol. (b) BF-TEM images of $Cs_2AgBiBr_6@SiO_2$ with different storage time (0, 1, and 48 h) in methanol. (c) XRD patterns of $Cs_2AgBiBr_6$ nanocrystals and $Cs_2AgBiBr_6@SiO_2$ stored in methanol for 48 h.

Table S1. The fitting parameters of the PL decay curves of $Cs_2AgBiBr_6$ and $Cs_2AgBiBr_6@SiO_2$ powders.

Sample	A_1	τ_1(ns)	A_2	τ_2(ns)	A_3	τ_3(ns)	τ_{avg}(ns)
$Cs_2AgBiBr_6$	1976.50	0.99	244.10	6.62	57.68	54.77	27.54
$Cs_2AgBiBr_6@SiO_2$	119.81	1.23	868.01	5.41	110.73	21.13	9.10

Table S2. Selectivity and production rate for photo-reduction CO_2 to CO over different metal halide perovskites based photocatalysts.

Photocatalysts	Reaction system	Light source	Production rates (μmol g^{-1} h^{-1})	Selectivity (%)	Stability (h)	Ref.
$Cs_2AgBiBr_6$@SiO_2	TEOA/water/acetonitrile	300 W Xe lamp (>420 nm)	**271.76**	**93.81**	**>15**	This work
$Cs_2AgBiBr_6$ QDs	TEOA/water/acetonitrile	300 W Xe lamp (>420 nm)	**204.5**	**90.23**	**2**	This work
$Cs_3Bi_2Br_9$ QDs	Gas–solid	300 W Xe lamp (AM 1.5G)	137.76	98.7	>20	10
Cs_2CuBr_4 QDs	Gas–solid	300 W Xe lamp (AM 1.5G)	148.98	–	>20	11
$CsPbBr_3$ QDs	Ethyl acetate/water	300 W Xe lamp (AM 1.5G)	4.3	99	>8	12
Fe: $CsPbBr_3$ NCs	Ethyl acetate/water	450 W Xe lamp 150mW cm^{-2}	3.2	–	>3	13
$CsPbBr_3$-Re(600)	Tolune/isopropanol	300 W Xe lamp (> 420 nm)	104.4	95	>3	14
$CsPbBr_3$ NCs/MXene	Ethyl acetate	300 W Xe lamp (≥ 420 nm)	26.3		>9	15
$CsPbBr_3$@TiO-CN	Ethyl acetate/water	300 W Xe lamp (≥ 400 nm)	12.9	–	>10	16
$FAPbBr_3$ QDs	Ethyl acetate/water	300 W Xe lamp 100mW cm^{-2}	181.3	–	>3	17
ZnSe-$CsPbI_3$	Toluene/isopropanol	300 W Xe lamp 100mW cm^{-2}	53.96	–	–	18
Cs_2AgBiI_6	Toluene	300 W Xe lamp (≥ 420 nm)	18.9	100	–	19

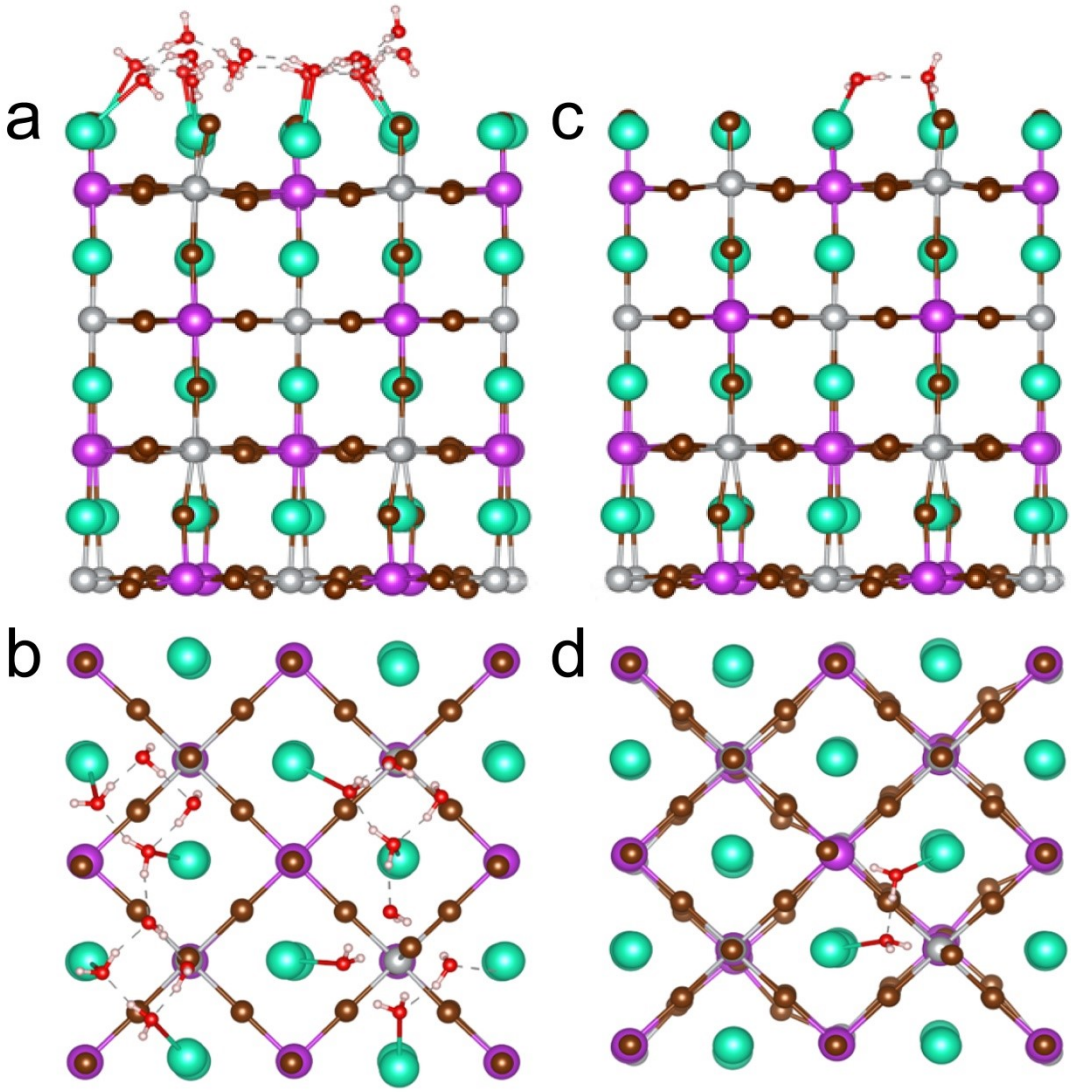

Figure S7. The optimized configuration of water adsorption on $Cs_2AgBiBr_6$ with the coverage of 1 ML (a, b) and 1/8 ML (c, d). Side-views and top-views are shown in the upper and lower panels, respectively.

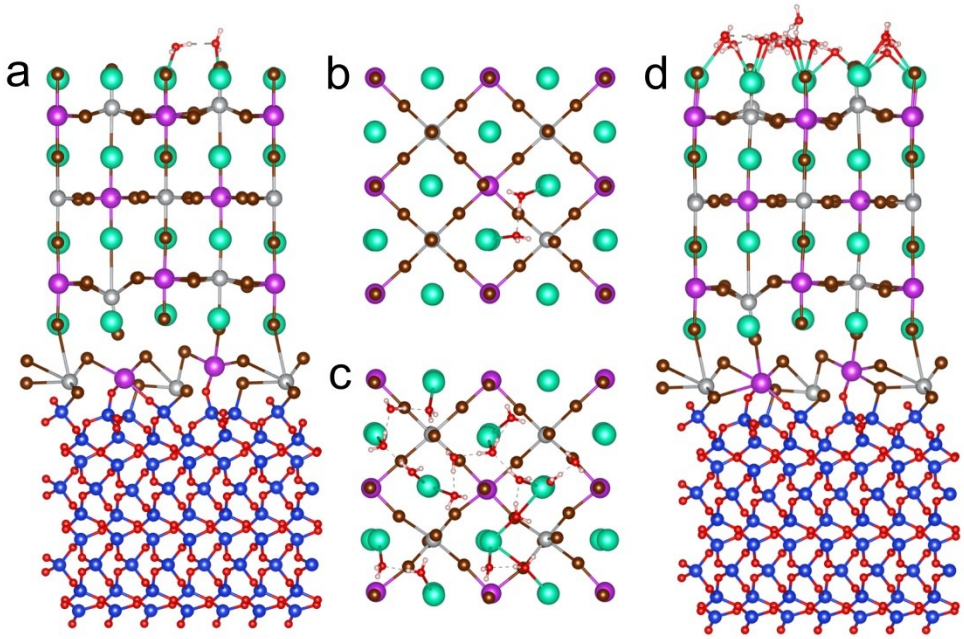

Figure S8. The optimized configurations of water adsorption on $Cs_2AgBiBr_6$-SiO_2 interface with the coverage of 1/8 ML (a, b) and 1 ML (c, d). Top-views are shown in the middle panel.

References

1 Z . Teng, X. Su, Y. Zheng, J. Sun, G. Chen, C. Tian, J. Wang, H. Li, Y. Zhao and G. Lu, *Chem. Mater.*, 2013, **25**, 98-105.

2 T. D. Kühne, M. Iannuzzi, M. D. Ben, V. V. Rybkin, P. Seewald, F. Stein, T. Laino, R. Z. Khaliullin, O. Schütt, F. Schiffmann, D. Golze, J. Wilhelm, S. Chulkov, M. H. Bani-Hashemian, V. Weber, U. Borštnik, M. Taillefumier, A. S. Jakobovits, A. Lazzaro, H. Pabst, T. Müller, R. Schade, M. Guidon, S. Andermatt, N. Holmberg, G. K Schenter, A. Hehn, A. Bussy, F. Belleflamme, G. Tabacchi, A. Glöß, M. Lass, I. Bethune, C. J. Mundy, C. Plessl, M. Watkins, J. VandeVondele, M. Krack and J.Hutter, *J. Chem. Phys.*, 2020, **152**, 194103.

3 J. P. Perdew, K. Burke and M. Ernzerhof, *Phys. Rev. Lett.*, 1996, **77**, 3865-3868.

4 S. Goedecker, M. Teter and J. Hutter, *Phys. Rev. B - Condens. Matter Mater. Phys.*, 1996, **54**, 1703-1710.

5 J.VandeVondele and J. Hutter, *J. Chem. Phys.*, 2007, **127**,114105.

6 S. Grimme, *J. Comput. Chem.*, 2006, **27**, 1787-1799.

7 P. Chen, Y. Huang, Z. Shi, X. Chen and N. Li, *Materials*, 2021, **14,** 2469.

8 B. H. Wang, B. Gao, J. R. Zhang, L. Chen, G. Junkang, S. Shen, C. T. Au, K. Li, M. Q. Cai and S. F. Yin, *Phys. Chem. Chem. Phys*., 2021, **23**, 12439-12448.

9 T. P. M. Goumans, A. Wander, W. A. Brown and C. R. Catlow, *Phys. Chem. Chem. Phys*., 2007, **9**, 2146-2152.

10 J. P. Sheng, Y. He, J. Y. Li, C. W. Yuan, H. W. Huang, S. Y. Wang, Y. J. Sun, Z. M. Wang and F. Dong, *ACS Nano*, 2020, **14**, 13103-13114.

11 J. P. Sheng, Y. He, M. Huang, C. W. Yuan, S. Y. Wang and F. Dong, *ACS Catal*., 2022, **12**, 2915-2926.

12 J. Hou, S. Cao, Y. Wu, Z. Gao, F. Liang, Y. Sun, Z. Lin and L. Sun, *Chem. – Eur. J*., 2017, **23**, 9481-9485.

13 S. Shyamal, S. K. Dutta and N. Pradhan, *J. Phys. Chem. Lett.* 2019, **10**, 7965–7969.

14 Z. C. Kong, H. H. Zhang, J. F. Liao, Y. J. Dong, Y. Jiang, H. Y. Chen and D. B. Kuang, *Solar RRL*, 2020**, 4**, 1900365.

15 A. Z. Pan, X. Q. Ma, S. Y. Huang, Y. S. Wu, M. J. Jia, Y. M. Shi, Y. Liu, P. Wangyang, L. He and Y. Liu, *J. Phys. Chem. Lett*., 2019, **10**, 6590-6597.

16 X. X. Guo, S. F. Tang, Y. F. Mu, L. Y. Wu, G. X. Dong and M. Zhang, *RSC Adv*., 2019, **9**, 34342-34348.

17 M. D. Que, Y. Zhao, Y. W. Yang, L. K. Pan, W. Y. Lei,W. H .Cai, H. D. Yuan, J. Chen and G. Q. Zhu, *Mater. Lett*., 2021, **282**, 128695.

18 N. Li, X. Chen, J. Wang, X. Liang, L. Ma, X. Jing, D. L. Chen and Z. Li, *ACS Nano*, 2022, **16**, 3332-3340.

19 D. F. Wu, X. S. Zhao, Y. Y. Huang, J. N. Lai, H. Y. Li, J. Y. Yang, C. Q. Tian, P. He, Q. Huang and X. S. Tang, *Chem. Mater*., 2021, **33**, 4971-4976.